Research Article

Adding value to natural clays as low-cost adsorbents of methylene blue in polluted water through honeycomb monoliths manufacture

M. Ahrouch[1,2] · J. M. Gatica[1] · K. Draoui[2] · H. Vidal[1]

Received: 17 July 2019 / Accepted: 5 November 2019 / Published online: 11 November 2019

Abstract
A natural Moroccan illite–smectite was used as an adsorbent for the removal of methylene blue (MB) from aqueous solutions. The clay was characterized by FTIR spectroscopy, TGA, SEM–EDS, X-ray fluorescence, XRD and N_2 physisorption. The influence of pH, temperature and time on the MB adsorption by the clay was investigated. The maximum equilibrium adsorption capacity was 100 mg g^{-1} at 45 °C. The kinetic behavior and the isotherms better-fitted with the pseudo-second-order and Langmuir models, respectively. Clay honeycomb monoliths (50 cells cm^{-2}) were obtained by means of extrusion from the starting material without any additive except water. The structured filters exhibited better performance under dynamic conditions than the powdered clay, adding value to the application of this low-cost adsorbent.

Keywords Adsorption · Clay · Honeycomb monolith · Methylene blue

1 Introduction

The releases of textile industry are in general loaded with organic micropollutants, in particular different detergents and dyes. The latter are often used in excess and can be classified according to their structure as anionic and cationic [1, 2]. In aqueous solution, anionic dyes carry a net negative charge due to the presence of sulfonate (SO_3^-) groups [3, 4], while cationic dyes carry a net positive charge due to the presence of protonated amine or sulfur-containing groups [5]. Due to their strong interaction with many surfaces of synthetic and natural fabrics [6], a broad variety of physicochemical and biological techniques has been developed and tested in the treatment of effluents loaded with these contaminants [7, 8]. These processes include precipitation, ionic exchange, filtration on membrane and irradiation. However, these processes are often expensive and lead to the generation of large quantities of sludges, in addition to the formation of compounds derived from the degradation of the active molecules, which are sometimes even more toxic [9, 10]. The accumulation and the low biodegradability of these compounds make the various treatments difficult to apply [11]. Among the wastewater treatment processes, adsorption remains a widely used approach for being easy to implement. The activated carbon is the adsorbent most largely employed, because of its great capacity of adsorption in agreement with its high specific surface area [12–14]. However, this adsorbent is expensive and poses the problem of its regeneration for a multiple use. The search for new effective and economic adsorbents thus proves attractive [15, 16]. In this context, the use of other adsorbent materials such as clays or natural zeolites is of great interest [17, 18].

The aim of our work was to optimize the adsorption performance of a natural argillaceous material, without any purification step, through its casting as structured filter for a possible replacement of the expensive adsorbents used in the polluted water treatment. In particular, we were interested in eliminating a cationic dye in aqueous solution by retention onto a local natural clay. Moreover, special attention was

✉ J. M. Gatica, josemanuel.gatica@uca.es | [1]Departamento C.M., I.M. y Química Inorgánica, Universidad de Cádiz, 11510 Puerto Real, Spain. [2]Laboratoire Matériaux et Systèmes Interfaciaux LMSI- Faculté des Sciences, Abdelmalek Essaâdi University, Tétouan, Morocco.

paid to the fabrication of honeycomb monoliths from this material and their further use for the same application, taking into account that most previous studies reporting on the use of clays to retain dyes employed powders [19–22], references dealing with clay structured filters being still comparatively scarce [23]. Let us also consider the advantages of the honeycomb monolithic design for the treatment of a high volume/flow, which are characteristic of environmental applications, in comparison with packed-bed reactors in which pressure drop may become a serious problem [24].

Here, we specifically report on the ability of an interstratified illite–smectite to eliminate methylene blue (MB) present in water. This clay was selected because in a previous study [25] it demonstrated to have a high adsorption capacity even of heavy metals such as lead. On the other hand, MB was chosen considering the vast literature available regarding the use of this organic dye in adsorption studies in liquid phase [26–31] with which we could compare our own results. Moreover, it was also selected according to its significant presence in the wastewaters proceeding from the local Moroccan textile industry. Undoubtedly, there are other colorant molecules that from an environmental viewpoint could be also interesting to adsorb such as methyl orange, malachite green, crystal violet, Congo red, rhodamine B, among others. However, MB is the most studied one as well illustrated by the fact that there are even reviews just focused on this dye [30, 31]. Since its discovery almost a century and half ago [27], MB is one of the most commonly used thiazine (cationic) dyes, and many different adsorbents have been reported for its removal from aqueous solutions [28]. Although it is not particularly hazardous, it has still some toxicity [29], and additionally, its quantitative detection is relatively simple. In this study, we first used a conventional batch-contact-time method [28], investigating the equilibrium of MB adsorption onto the powdered interstratified illite–smectite and fitting the data to the most used models (Langmuir, Freundlich) and also to the less employed Sips equation. The uptake of MB on the clay was examined as a function of adsorbate concentration, pH, adsorption temperature and contact time. Furtherly, honeycomb monoliths were also manufactured from the starting clay powder and tested in the retention of methylene blue under dynamic conditions via recirculated plug-flow adsorption experiments. This study was performed in order to add value to these low-cost adsorbents and to investigate their potential for a real application.

2 Materials and methods

2.1 Materials

The clay used in this study as dye adsorbent was an interstratified illite–smectite collected from the north region of Morocco known as Chefchaouen. It had a CEC of 63 mEq/100 g as measured by the well-known cobalt (III)-hexamine trichloride method [32].

The basic dye used in this study was methylene blue (MB), from Fluka, with $C_{16}H_{18}C_lN_3S \times 3H_2O$ chemical formula which is of analytical grade. This cationic dye model presents decentralized positive charge on the organic framework, which could play a major role in keeping the species on the surface of the clay, the wavelength of 664 nm corresponding to its maximum absorbance [28]. Literature on the MB adsorption by clays is certainly vast, and it has even been used as a method to evaluate CEC and surface areas of clays [31–33]. In this research, working solutions of MB were prepared with deionized water and from a stock solution of 500 mg L^{-1} to give the required initial concentrations (C_0 = 20–500 mg L^{-1}) for each experimental run [34].

2.2 Clay monoliths preparation

The clay honeycomb monoliths were obtained by extrusion of a paste, previously prepared by mixing the initial fine starting powder (< 10 µm) with the adequate amount of water (51 mL g^{-1} of paste). The extrudability of this paste, which did not require extra additives, was first predicted according to Casagrande's technique as it exhibited appropriate rheological parameters such as a liquid limit and a plasticity index of 50% and 29.6%, respectively [35]. The resulting green monoliths were dried overnight at 60 °C and subsequently calcined at 450 °C for 4 h. This treatment was chosen from thermogravimetric analysis results (see below) as the one allowing optimal enhancement of the mechanical resistance while preserving the clay structure, as learned from the previous experience with other clays [36]. The final monoliths presented a honeycomb-type circular section with a diameter of 1.4 cm, a density of approx. 50 cells cm^{-2}, 0.33 mm of wall thickness and a 72% open frontal area (Fig. 1).

2.3 Characterization of the adsorbents

XRF compositional analysis of the starting clay was carried out in a Bruker S4 Pioneer spectrometer.

The textural characterization was performed by means of N_2 physisorption at −196 °C using an automatic Autosorb IQ (Quantachrome) analyzer. The clay samples (both in the form of powder and as honeycomb monoliths) were degassed at 150 °C for 2 h. The obtained isotherms were used to calculate their specific surface area (S_{BET}) and micro- and mesoporosity. Total pore volume (V_p) data were calculated from the amount of nitrogen adsorbed at a 0.97

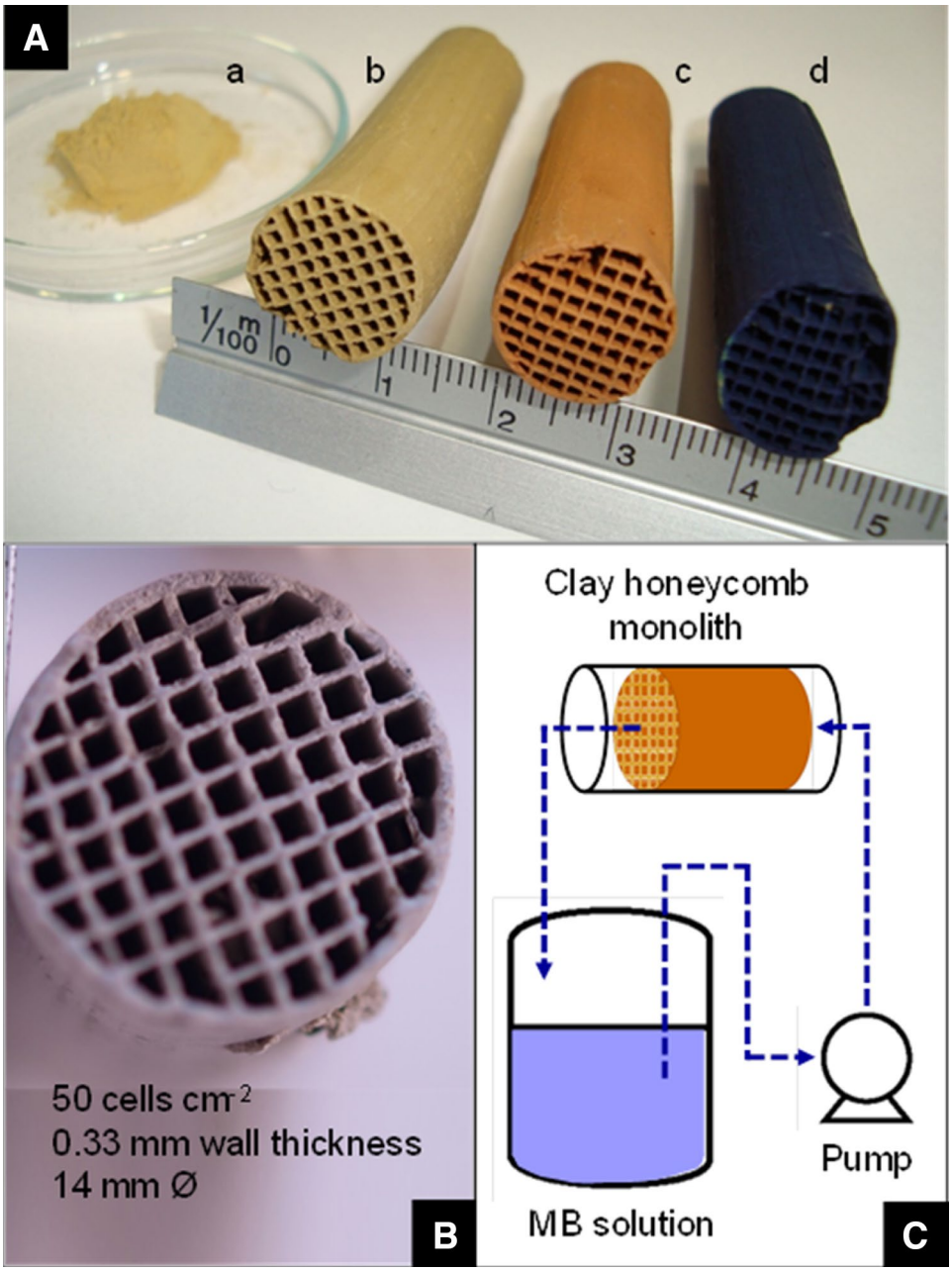

Fig. 1 **A** Image of the starting clay powder (a) and clay honeycomb monoliths prepared from it after simple extrusion plus drying (b), additional calcination at 450 °C for 4 h (c) and further use to adsorb methylene blue (d); **B** geometric characteristics of the clay honeycomb monoliths; and **C** schematic diagram of the experimental setup for the dynamic adsorption studies, in which a centrifugal pump was employed

relative pressure value (P/P_0). Pore size distribution and the average pore were examined by the BJH method from the desorption branch of the isotherms.

The FTIR spectra in transmission mode were obtained using a Thermo vertex 70 FTIR spectrophotometer. About 1 mg of sample clay was mixed with approximately 200 mg of dried KBr to get pellets. Measurements were taken over the range 4000–400 cm^{-1} in the absorbance mode, with a spectral resolution of 4 cm^{-1}. This technique was employed to study the clay samples both before and after the MB adsorption.

The thermogravimetric analysis (TGA) was carried out under air in a Shimadzu TGA-50 thermobalance over 50 mg of powdered samples using a heating rate of 10 °C min^{-1}.

SEM images and EDS compositional data of the clay powder were obtained using a QUANTA-200 scanning electron microscope equipped with a Phoenix microanalysis system using a nominal resolution of 3 nm. SEM images of the clay calcined at 450 °C for 4 h and of the clay monolith after the same treatment were acquired in a field emission gun (FEG) scanning electron microscope (Nova NanoSEM 450).

XRD studies were carried out in a Bruker diffractometer, D8 Advance 500 model. Diffractograms were recorded using CuKα radiation, and the 2θ angle ranged from 1.5° to

75°, with a step of 0.017° and a counting time per step of 1 s. Refinement of the analysis was performed by applying a Rietveld method by means of the FullProf program [37]. In addition, semiquantitative analysis of the mineralogical composition was made by means of the PowderCell 2.4 software.

2.4 Batch adsorption experiments

The adsorption of MB over the fresh clay powder was studied in a batch equilibration system. Different parameters including initial concentration of MB, contact time, stirring speed and pH of the MB solutions were adjusted, the latter by adding 0.1 N HNO_3 or 0.1 N NaOH solutions. In general, the adsorption experiments were carried out by varying the initial concentrations from 50 to 500 mg L^{-1}. In each case, 0.2 g of sample was added to a conical flask which contained the MB solution (50 mL). Two types of experiments were performed. First, the adsorption kinetic curves for two initial concentrations of MB (200 and 300 mg L^{-1}) were obtained at room temperature in order to study the effect of contact time (1 min–4 h) on the adsorption of MB on the clay. The suspensions were continuously shaken at 150 rpm, and the experimental data were examined by pseudo-first-order and pseudo-second-order kinetics [38, 39]. For the fitting, only data up to saturation (approx. 30 min) were considered. In the second type of experiments, the suspensions were stirred at the same speed as before during 4 h (considering the results from the kinetic study) under variable temperature conditions (20, 25, 35 and 45 °C). The adsorption experiments were carried out in a closed system. The MB solutions were kept in thermal equilibrium using an automatic thermostat system, including a water bath and an integral shaker drive. Three theoretical isotherm models, Langmuir, Freundlich and Sips [25], were considered to fit the experimental data.

In all cases, the remaining MB in balance was analyzed by UV–visible spectrophotometry. The amounts of MB adsorbed were calculated from the difference between initial and final or equilibrium concentration of the corresponding solutions.

2.5 Dynamic adsorption experiments

The capacity to adsorb MB by the clay honeycomb monoliths was studied at room temperature in a homemade system (Fig. 1), using approx. 6.5 g weighted monoliths ($L = 5.2$ cm approx.) and a 1200 cm^3 min^{-1} recirculated flow of the MB aqueous solution (1 L). This study allows testing the potential application of the monoliths in the treatment of polluted liquid effluents under more realistic conditions. Experimental conditions (mass of adsorbent and dye concentration) were different to those selected for the batch experiments because the two types of experiments are not comparable. In order to make a comparison with the powder, a packed column containing the same quantity of powdered clay ($Ø = 1.5$ cm, $L = 2.5$ cm), with quartz wool at the outlet to avoid powder drag, and previously submitted to the same calcination treatment as the monolith (450 °C, 4 h), was also tested in the same experimental setup of the monolith. Blank experiments confirmed previously a negligible MB adsorption over the quartz wool. In both cases, column and monolith, two different initial concentrations of MB, were studied: 20 and 100 mg L^{-1}. As for the batch experiments, the adsorption capacity was analyzed by measuring the absorbance at 664 nm of the residual liquid phase, after filtration, in a UV–visible Cary 50 spectrophotometer from Varian.

3 Results and discussion

3.1 Sample characterization

The chemical composition of the employed natural clay as estimated by XRF analysis is given in Table 1. It is remarkable that it resembles that typically exhibited by other smectite- and illite-type minerals with predominant presence of silicon, aluminum and iron oxides [40, 41].

The clay FTIR spectrum is presented in Fig. 2. The sharp band at 3625 cm^{-1}, the broad shoulder at 3420 cm^{-1} and the small peak at 1630 cm^{-1} are attributable to the framework OH groups stretching, interlayer water OH stretching and H_2O deformation band typically observed in many smectites [42]. Silanol groups (Si–OH) are therefore spread over the clay surface. This is a very active surface group, which could interact with polar organic compounds as methylene blue during the adsorption process [43]. On the other hand, the most intense bands are perfectly understandable in terms of clay lattice vibrations, some of which are of the same nature as those of quartz (Si–O–Si or O–Si–O vibrations) [44], except the small peak at 1384 cm^{-1} which might correspond to some carbonates [45]. Their presence in any case must not be significant considering the relative low intensity of the mentioned peak [40, 41]. Figure 2 also shows that calcination

Table 1 X-ray fluorescence analysis of oxide content (wt%) for the clay sample investigated

SiO_2	Al_2O_3	Fe_2O_3	Cr_2O_3	MgO	CaO	K_2O	TiO_2	V_2O_5	SO_3	ZnO	SrO
60.4	21.5	6.8	< 0.1	1.2	2.2	2.0	1.1	< 0.1	0.1	< 0.1	< 0.1

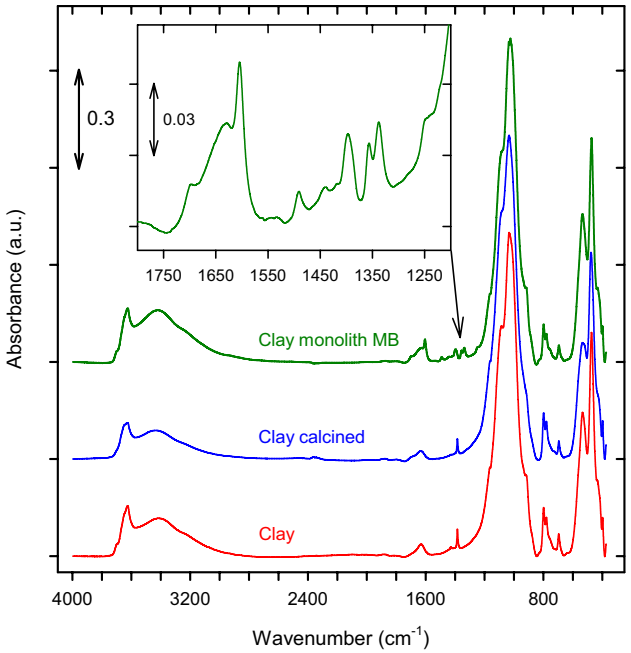

Fig. 2 FTIR spectra corresponding to the powdered clay sample, both fresh and calcined at 450 °C for 4 h, and crushed pieces of the clay honeycomb monolith after MB adsorption. Details of the MB adsorption IR bands are shown in the inset

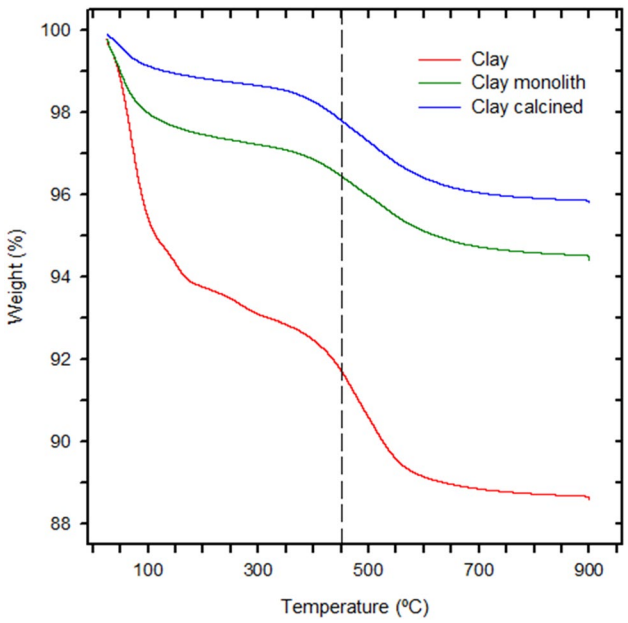

Fig. 3 TGA profiles of the clay sample as-received, after calcination at 450 °C for 4 h, and after extrusion as a honeycomb monolith plus calcination at 450 °C for 4 h. The dashed line indicates the temperature at which a waterproof monolith can be obtained

of the clay at 450 °C for 4 h, the thermal treatment applied to the clay honeycomb monoliths as the last step of their preparation to make them waterproof, hardly modifies the infrared spectrum. Only a slight decrease in the bands above 3000 cm^{-1} is observed, what can be denotative of some dehydroxylation and dehydration of the clay [42].

The thermal stability of the fresh clay, the clay calcined at 450 °C for 4 h and the clay-based monolith submitted to the same treatment was also studied. As shown in Fig. 3, the thermal analysis reveals the existence of two main different stages of weight loss for the fresh clay. The first loss occurs practically from room temperature up to approximately 200 °C and might reasonably correspond to the release of adsorbed water. The second weight loss, which extends up to around 600 °C, should be basically related to dehydroxylation of the different silicate phases present in the clay, not discarding some contribution of interlayer water. In the case of the calcined sample, there is a reasonable decrease in the weight loss with almost complete disappearance of the first stage. Finally, the slightly higher mass loss in the clay honeycomb monolith if compared to the latter is attributable to a higher humidity degree reached from exposure to the air after the calcination treatment. In any case, the similarity of its profile respect to the calcined powder suggests that the extrusion process has no effect on the composition or structure of the clay. Moreover, the thermogravimetric analysis also points to the suitability of the calcination treatment at 450 °C for leading to a monolith that is resistant to the aqueous phase while mostly preserving the initial clay.

The XRD study gave results in agreement with the above. As can be observed in Fig. 4, the diffractogram of the raw clay can be interpreted as the sum of contributions of different phases. In particular, the relatively most intense peaks can be assigned to quartz (most likely present as large crystals), in good agreement with the FTIR analysis, while the rest is mainly associated with an interstratified silicate composed of illite–muscovite and smectite–montmorillonite and with topaz. The presence of all these hydroxylated silicate minerals is also consistent with the TGA study above commented. Moreover, the Rietveld analysis indicated that the best-fitting of the experimental data is obtained when other minority phases are considered such as lazurite, zircon, rutile, albite, boehmite, anatase, gibbsite, augelite, glauberite and glauconite. The presence of these phases, although much less significant, might justify the content of elements such as Al, Fe, Mg, Ca, K, Ti or S measured by XRF (Table 1). In addition, the semiquantitative analysis allowed estimating the mineralogical composition of our clay as follows: 43.0% smectite, 23.8% illite, 30.2% quartz and 2.9% topaz. This confirms that the contribution of impurities, on the other hand, is reasonable for a natural clay that has not been treated/purified with the intention to simplify the overall manufacture of our low-cost adsorbent filters. It is also remarkable

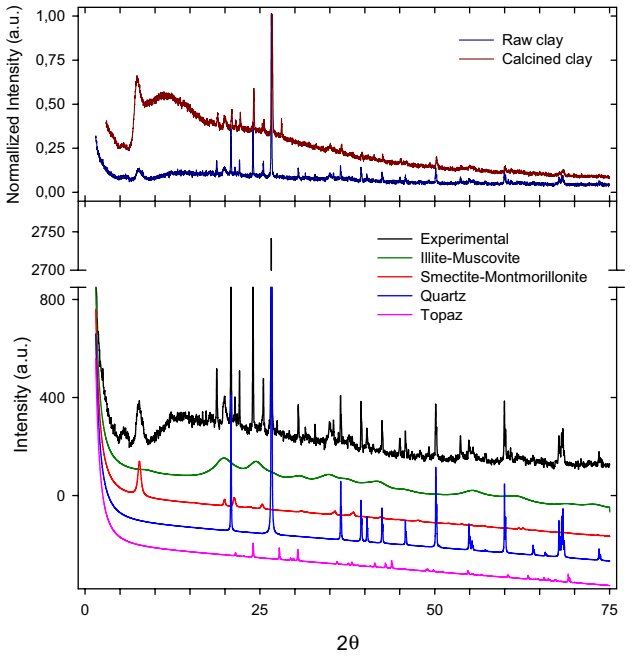

Fig. 4 Normalized X-ray diffractograms obtained for the clay as-received and after calcination at 450 °C for 4 h (upper part), and experimental X-ray diffractogram of the raw clay along with its main phases detected according to Rietveld analysis, their Y-axis position being displaced for the sake of clarity (lower part). Structural data for the Rietveld analysis were obtained from the Inorganic Crystal Structure Database (ICSD) and Crystallographic Open Database (OCD) as follows: illite–muscovite, ICSD 63123; smectite–montmorillonite, COD 9002779; Quartz, ICSD 63532; Topaz, ICSD 72938

that the analysis of the diffractogram obtained for the calcined clay (upper part of Fig. 4) was similar to that of the fresh clay, so confirming that the calcination treatment did not significantly alter the structure of the clay.

The N_2 adsorption–desorption isotherms and BJH pore size distribution curves of both clay powder and clay honeycomb monoliths are plotted in Fig. 5. Curves corresponding to the clay powder calcined at the same temperature as the monolith are also included as a reference. All the isotherms showed the typical II-type sorption behavior, characteristic of mainly macroporous adsorbents according to the IUPAC classification, with H3-type hysteresis loop denotative of plate-like particles giving rise to slit-shaped pores [46]. On the other hand, the BET surface area and pore volumes were calculated from the adsorption data, the values being summarized in Table 2. As expected, the calcination treatment induces some decrease in porosity and consequently of specific surface area. On the contrary, extrusion of the clay has almost no effect on the textural properties, since the values obtained for the calcined powder and honeycomb monolith are very similar. It should be also noticed that all the samples, although mainly macroporous, have some meso- and microporosity, put into evidence by the pore size distribution curves of Fig. 5.

Finally, Fig. 6 shows a representative SEM image (a) and its corresponding EDS spectrum (b) obtained for the fresh clay sample. As can be noticed, the clay is composed of an agglomerate of particles of heterogeneous size and irregular shape. It is also displayed inter-particle/agglomerate void spaces that may contribute to porosity as stated above. The look resembles very much that observed previously for other natural clays of smectite type [36, 40, 41].

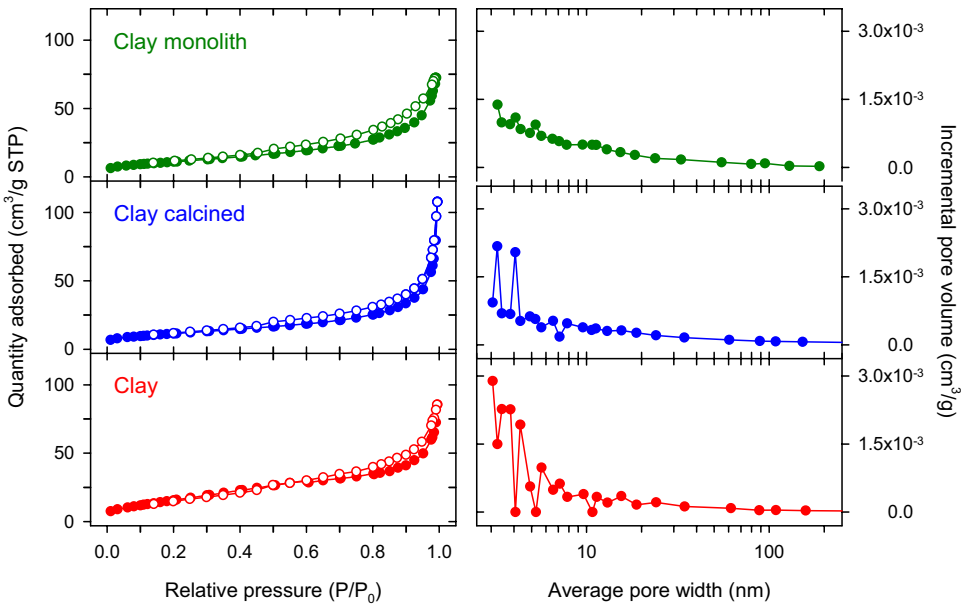

Fig. 5 N_2 adsorption–desorption isotherms and pore size distribution curves of the clay sample as-received, after calcination at 450 °C for 4 h, and after extrusion as a honeycomb monolith plus calcination at 450 °C for 4 h

Table 2 Textural data of the investigated samples as estimated from N_2 physisorption

Sample	S_{BET} ($m^2\ g^{-1}$)	Total pore volume ($cm^3\ g^{-1}$)	Micropore volume ($cm^3\ g^{-1}$)
Fresh clay	61	0.093	0.021
Calcined clay[a]	41	0.087	0.018
Clay-based monolith[a]	40	0.086	0.019

[a]Both calcined at 450 °C for 4 h

In the same way, similar images were obtained for the calcined powder (Fig. 6c), demonstrating that no significant morphological changes occur as a result of the calcination treatment. Regarding the clay monolith, the apparent loss of surface roughness in the images obtained for this sample (Fig. 6d) can be reasonably attributed to the higher compaction of the clay grains as a result of the extrusion step. Also noticeable, except gold that is present due to its use for metalizing the raw clay sample, all the elements detected by EDS analysis are consistent with both the XRF analysis and XRD study above discussed.

3.2 Adsorptive performance of the powdered clay

3.2.1 Effect of pH

The effect on the MB adsorption by the studied clay at varying the solution pH is shown in Fig. 7a. The results indicate that the dye removal efficiency slightly increases between pH values of 2 and 8. A similar trend was observed by other authors studying the adsorption of MB on different natural clays of smectite [28, 47] or diatomite [43] type, but it contrasts with results obtained for kaolin [18]. It is also noteworthy that the adsorption capacity of our adsorbent increased remarkably above pH 8, especially with increasing the pH value from 10 up to 12. In

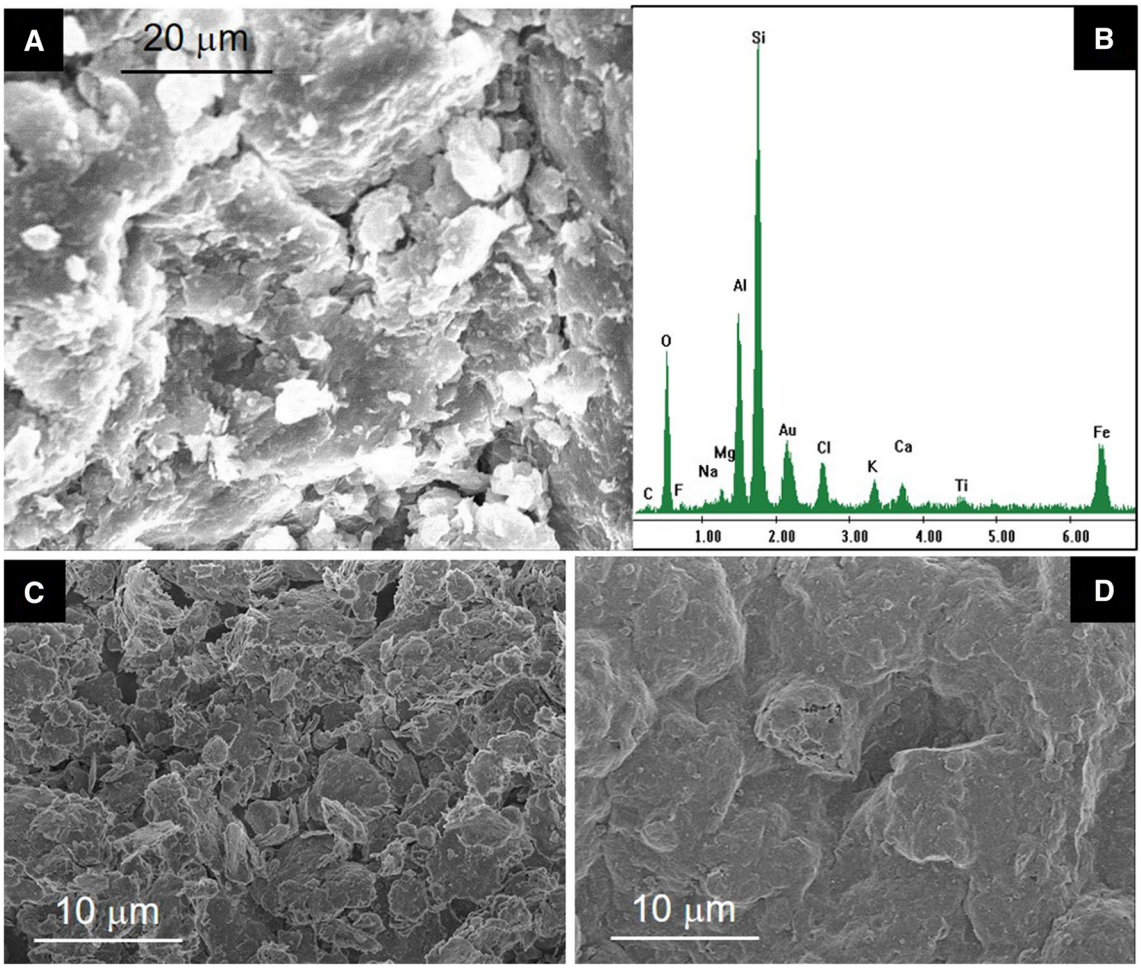

Fig. 6 SEM image (**a**) and EDS spectrum (**b**) of the fresh clay powdered sample, and SEM images of the clay calcined at 450 °C for 4 h (**c**) and the clay honeycomb monolith calcined at the same conditions (**d**)

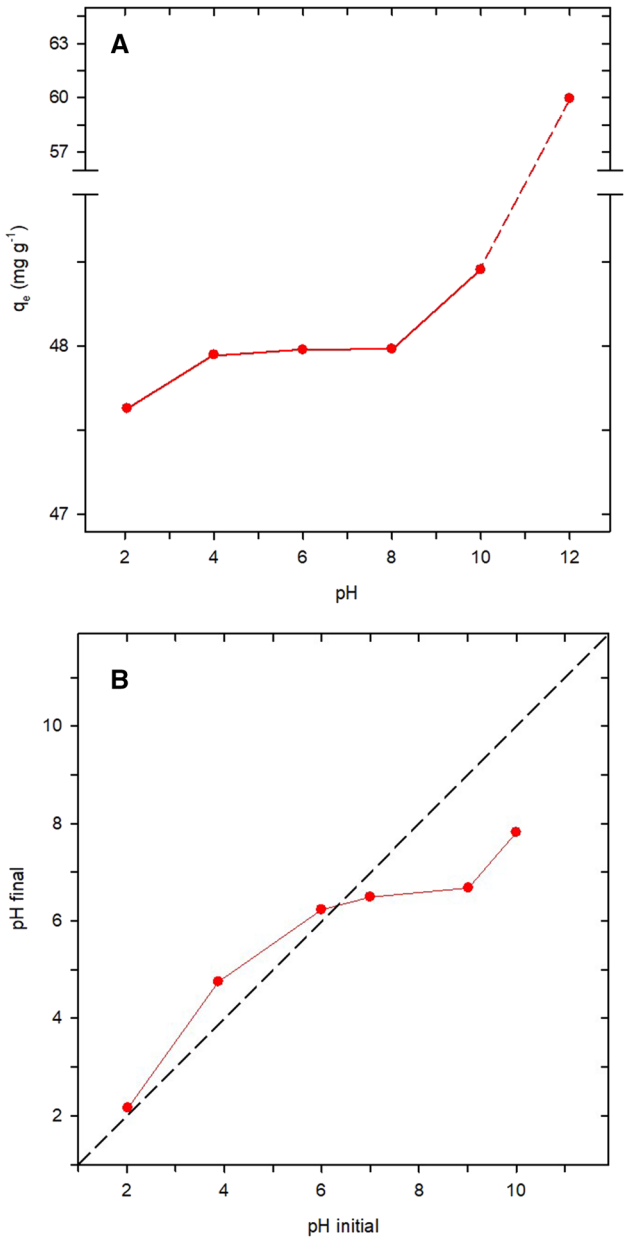

Fig. 7 **a** Effect of pH on the adsorption of MB (initial concentration = 240 mg L^{-1}, stirring speed = 150 rpm, temperature = 25 °C, contact time = 240 min and adsorbent dosage = 0.1 g/25 mL); **b** determination of the point of zero charge (pzc) value for the clay sample. The intersection of solid and dashed lines indicates the pH values at which the pH of the dye solution before (pH_i) and after (pH_f) the contact with the clay is the same

order to understand this dependence of the MB adsorption with the pH, we performed additional measurements to estimate the point of zero charge (pzc) of the studied clay sample which resulted to be 6.4, observing that the surface of the adsorbent becomes negatively charged, especially above pH 8 (Fig. 7b). This effect can explain why

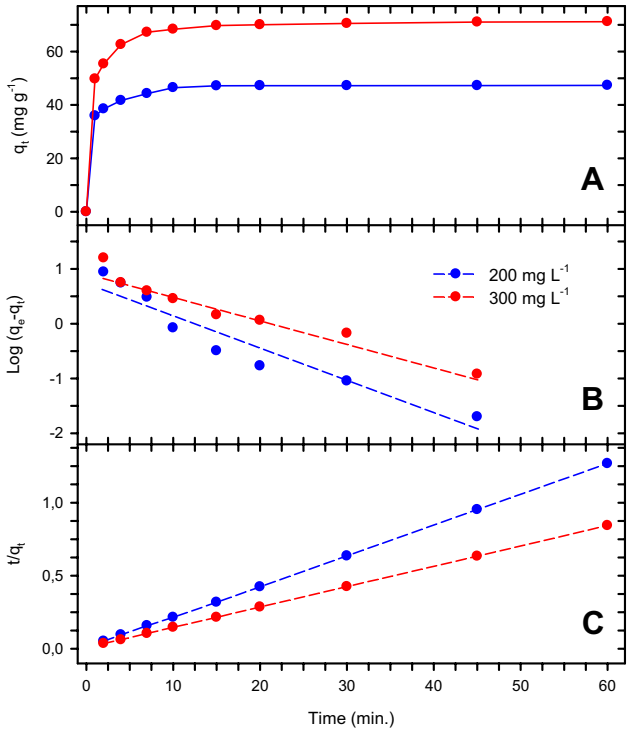

Fig. 8 Adsorption kinetics curves for the adsorption of MB on the clay sample at room temperature (**a**). The maximum percentage of MB removal corresponding to the initial concentrations of 200 mg L^{-1} and 300 mg L^{-1} was 25% in both cases. The figure also includes kinetic modeling to a pseudo-first-order (**b**) and to a pseudo-second-order (**c**)

above this value the electrostatic interaction with the MB cationic molecule is particularly favored [13].

3.2.2 Adsorption kinetics

Figure 8a shows the MB adsorption capacity of our clay at room temperature as a function of time under the dye initial concentrations of 200 mg L^{-1} and 300 mg L^{-1}. Notice that the adsorption process was rapid in the first minute, then continued with a slower rate during the following 10 min, and finally reached a nearly constant value after 30 min.

As previously mentioned in the experimental section, the results were analyzed by using the models of pseudo-first-order and pseudo-second-order [48, 49]. The rate constants of the MB adsorption on the clay were determined graphically (Fig. 8b, c), leading to the results summarized in Table 3. The highest correlation coefficient, that denotes the best-fitting of the experimental data, was found for a pseudo-second-order model. This result agrees with many previous studies that employed not only natural clays [18, 21, 28, 47, 50] but also other proposed synthetic materials such as activated carbons from biomass [13, 16],

Table 3 Kinetic parameters for the adsorption of MB on the clay sample

C_0 (mg L^{-1})	q_e exp (mg g^{-1})	Pseudo-first-order			Pseudo-second-order		
		k_1 (min^{-1})	q_e cal (mg g^{-1})	R^2	k_2 (g mg^{-1} min^{-1})	q_e cal (mg g^{-1})	R^2
200	47.3	0.139	5.8	0.902	0.054	47.6	0.999
300	71.2	0.097	9.4	0.934	0.029	71.4	0.999

oxides [15] and silicates [19]. In addition, Table 4 shows the pseudo-second-order model constant rate values reported for different adsorbents allowing a comparison with our own results.

3.2.3 Adsorption isotherms

The adsorption isotherms were obtained by monitoring the evolution of the retention capacity at equilibrium, q_e (mg g^{-1}), for each initial concentration of the pollutant as function of the equilibrium concentrations (mg L^{-1}) at different temperatures (20, 25, 35 and 45 °C). The obtained results are plotted in Fig. 9a.

The experiments carried out show that the capacity of adsorption increases with the initial concentration. In addition, the shape of the obtained isotherms suggests the saturation of the surface sites and therefore the formation of the monolayer. A similar trend was found by other authors when studying MB adsorption on different natural clays [18, 43, 47]. Moreover, according to Giles classification [51], our isotherms, with independence of the temperature studied (20–45 °C), are of type H which are the result of the dominance of strong ionic adsorbate–adsorbent interactions [52]. In this sense, a chemical adsorption of positively charged functional groups of MB on the negatively charged surface groups of the clay is proposed.

Fitting of adsorption isotherms of MB on the clay sample by the Langmuir model was also studied by plotting C_e/q_e versus C_e. According to Fig. 9b, the values obtained in such representation follow an almost perfect linear trend what indicates that the Langmuir model is adequate for a good description of our adsorption isotherms. From the above data, monolayer adsorption capacities were estimated in each case, resulting to be 100, 95, 94 and 92 mg g^{-1} at 45, 35, 25 and 20 °C, respectively. The relatively small dispersion of these values in the studied range suggests that the temperature has not a great effect on the adsorption capacity. It is remarkable that the maximum adsorption capacity measured in this study (100 mg g^{-1}) is an intermediate value in the context of adsorption capacities for natural materials [31]. Moreover, our result is higher than that reported for other natural clays [21], low-cost recycled wasted materials from tea or rice [15], or even similar to that of more sophisticated adsorbents with clearly higher specific surface area, either activated carbon-based [15] or mesoporous silicates [19]. Additionally, Table 5 summarizes the maximum adsorption capacity values reported for other adsorbents in the literature. Comparing them with the results obtained in this work, our Moroccan illite–smectite can be employed as low-cost adsorbent and considered as an alternative to other materials such as activated carbon and mesoporous silicate for the MB removal.

Table 4 Parameters determined by theoretical models for the adsorption of MB over different adsorbents

Adsorbent	K_2 (g mg^{-1} min^{-1})[a]	K_L (L mg^{-1})[b]	ΔG° (KJ mol^{-1})	References
Activated carbon	–	0.04/0.07	–	[13]
Mesoporous birnessite	–	0.27/0.44	−4.3/−8.8	[15]
Activated carbon	0.057	0.03	−7.9/−12.4	[16]
Kaolin and zeolite	0.014/0.63	–	81.5/88.5	[18]
Mesoporous silicate material (dolomite)	0.0001/0.0007	0.12/0.18	−0.3/−4.5	[19]
Natural serpentine	0.001	0.05	−0.3/−3.0	[21]
Montmorillonite	0.004/0.042	0.01/0.77	–	[28]
Moroccan clays	0.003/0.13	0.27/2.12	−7.0/1.4	[46]
Moroccan diatomite	0.015	1.30	−30.8/−35.3	[47]
Natural clay mineral	–	−0.07/−0.03	6.8/7.4	[51]
Natural Moroccan illite–smectite	0.029/0.054	1.11/1.91	−32.7/−33.7	This work

[a]Pseudo-second-order

[b]Langmuir model

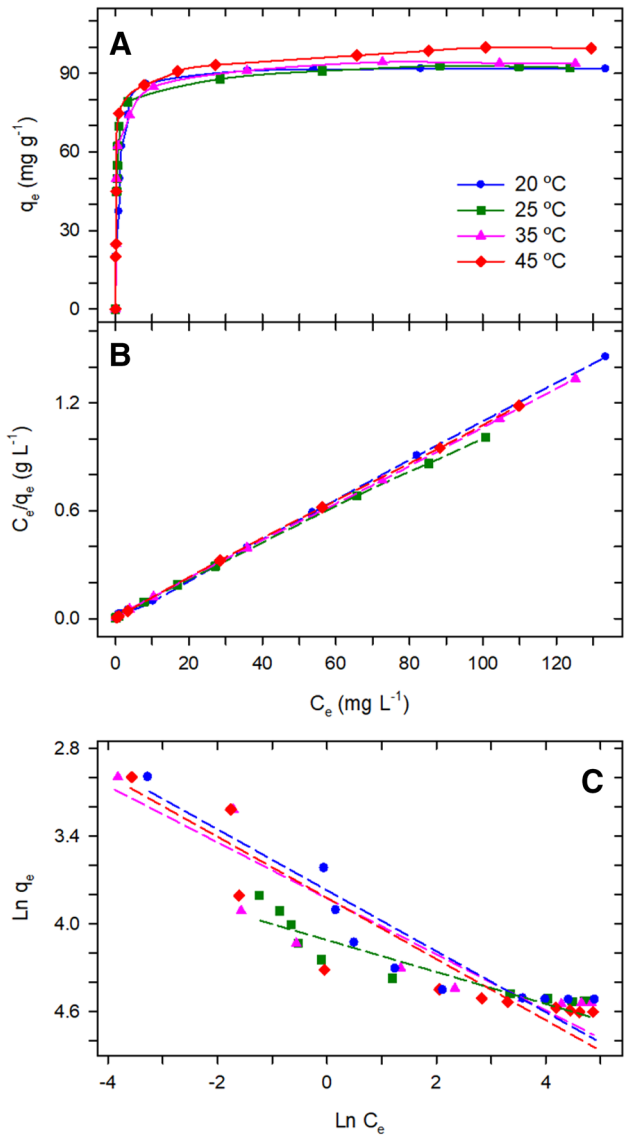

Fig. 9 Adsorption isotherms and effect of the temperature of the MB solution in contact with the clay sample (**a**); fitting of the isotherms data to a Langmuir model (**b**); and fitting of the isotherms data to a Freundlich model (**c**)

The results of fitting the adsorption isotherms to the Freundlich model are represented in Fig. 9c. On the other hand, the parameters values of Langmuir, Freundlich and Sips models are summarized in Table 6. Their comparison allows concluding that the experimental data fit better with the Langmuir model, according to the respective correlation coefficients (R^2). Such conclusion agrees with that of other authors who also found that data corresponding to MB adsorption onto different natural clays were better described by the Langmuir isotherm model [21, 28, 43, 47], being their corresponding constant values in a reasonably similar range (Table 4). Additionally, the results found in this work suggest that MB adsorption occurs like a monolayer on homogeneous sites, which are identical and contain equivalent energy [13].

Table 5 Maximum adsorption capacity of various adsorbents for MB according to Langmuir model

Adsorbent	q_{max} (mg/g)	References
Mesoporous birnessite	113	[15]
Kaolin and zeolite	45–22	[18]
Mesoporous silicate material (dolomite)	92	[19]
Natural serpentine	58	[21]
Raw kaolin	14	[33]
Moroccan raw and decanted clays	49–114	[46]
Moroccan diatomite	11	[47]
Natural clay mineral	76	[51]
Raw ball clay	34	[52]
Modified ball clay	100	[52]
Natural Moroccan illite–smectite	100	This work

Table 6 Langmuir, Freundlich and Sips parameters for MB adsorption by the clay sample

	T (°C)	20	25	35	45
Freundlich model	K_F (mg g^{-1})	45.6	60.4	48.9	48.5
	$1/n$	0.186	0.100	0.168	0.181
	R^2	0.863	0.862	0.826	0.849
Langmuir model	Q_m (mg g^{-1})	91.7	93.5	95.2	100.0
	K_L (L mg^{-1})	1.91	1.89	1.41	1.11
	R^2	0.999	0.999	0.999	0.999
Sips model	Q_m (mg g^{-1})	97.93	92.0	92.5	99.5
	K_S (L mg^{-1})	1.04	2.87	3.60	2.11
	n	0.68	0.89	1.01	0.71
	R^2	0.961	0.982	0.918	0.958

3.2.4 Adsorption thermodynamics

Thermodynamic studies are especially useful for interpreting the adsorption behavior in terms of process equilibrium [48]. Thermodynamic parameters evidencing the influence of temperature can be determined by combining the thermodynamic equation, $\Delta G° = \Delta H° - T\Delta S°$, and van't Hoff equation, which allows achieving the Eyring equation (Eq. 1):

$$\mathrm{Ln}\left(k_e^\circ\right) = \frac{-\Delta H^\circ}{RT} + \frac{\Delta S^\circ}{R} \quad (1)$$

where R is the universal gas constant (8.314 J K^{-1} mol^{-1}), T (K) the absolute temperature, k_e° is the thermodynamic equilibrium constant, and $\Delta H°$ and $\Delta S°$ are the changes in enthalpy and entropy, respectively. Therefore, in this work the thermodynamics of the MB adsorption onto the clay

was also investigated at different temperatures, in particular at 20, 25, 35 and 45 °C. According to the latest estimates of different authors [53, 54] to determine thermodynamic parameters, the right way to calculate the equilibrium constant for the adsorption system includes obtaining adsorption isotherms at different temperatures. In this context, it is recommended to use the equation described below (Eq. 2) to determine the thermodynamic parameters:

$$K_e^\circ = \frac{1000 \cdot K_L \cdot \text{molecular weight of adsorbate} \cdot [\text{adsorbate}]^\circ}{\gamma} \quad (2)$$

where K_e° is the thermodynamic equilibrium constant that is dimensionless, K_L is the Langmuir isotherm constant, [adsorbate]° is the standard concentration of the adsorbate (1 mol L^{-1}), and γ is the activity coefficient which is unitary for very diluted or ideal solutions. The average standard enthalpy change of MB adsorption on the clay was estimated using the above equation. The values of ΔS° and ΔH° were obtained from the intercept and slope of the plot of ln (K_e°) against 1/T (Fig. 10), resulting to be 45.1 J K^{-1} mol^{-1} and − 19.5 kJ mol^{-1}, respectively, what leads to values of the change in free energy ($\Delta G°$) around − 33 kJ mol^{-1} in the range of 20–45 °C (Table 7), with a correlation coefficient for the fitting of 0.994. Therefore, the process of MB adsorption on the clay here studied is exothermic [49, 55] and spontaneous. Our results contrast with those obtained by other authors [18, 28, 43] who found positive values for both $\Delta H°$ and $\Delta S°$ in the case of the adsorption of MB onto a natural montmorillonite, kaolin or diatomite, respectively. On the contrary, our results agree with those reported for the same process over two other clay minerals, one of them mainly composed of quartz, clay, dolomite, hematite and feldspars, and the other consisting of illite associated with very small amounts of chlorite [47]. In any case, it should be noticed that establishing a correlation between thermodynamics of the adsorption process and the mineralogical nature of the clay used as adsorbent is not certainly an easy task. This finding is well illustrated by Omer et al. [56] in a recent paper, in which both, the exo- or endothermic characters, could be observed for a same type of mineral category. This is also reflected on the wide range of values estimated for $\Delta G°$ as illustrated in Table 4.

3.3 Methylene blue adsorption on the clay honeycomb monolith

After studying the retention of MB on our clay as a powder, we conducted an additional study using it in the form of honeycomb monolith but under dynamic conditions (Fig. 1). Evidences for the MB adsorption on the clay monolith were obtained not only from its coloring after the process (Fig. 1) but also through FTIR analysis of crushed pieces (Fig. 2). As it can be observed, new peaks at 1602, 1486, 1393, 1353 and 1333 cm^{-1} were detected after the dye was adsorbed. The first two can be assigned to C=C and C=N, and $C=S^+$ stretching vibrations of the MB heterocycle, respectively, while those at lower frequency might be associated with the symmetrical and asymmetrical bending vibrations of the CH_3 functional groups of MB and the stretching vibrations of the C–N terminal saturated dimethylamino groups [56, 57]. It should be added that the position of the peaks previously attributed to the clay was not shifted as a consequence of the interaction with MB. This is consistent with the electrostatic nature of the interaction between adsorbate and adsorbent above suggested by the isotherms. It is also reasonable considering that our clay was not functionalized to enhance its adsorptive performance as other authors did [22]. The only significant change observed after the treatment with MB is

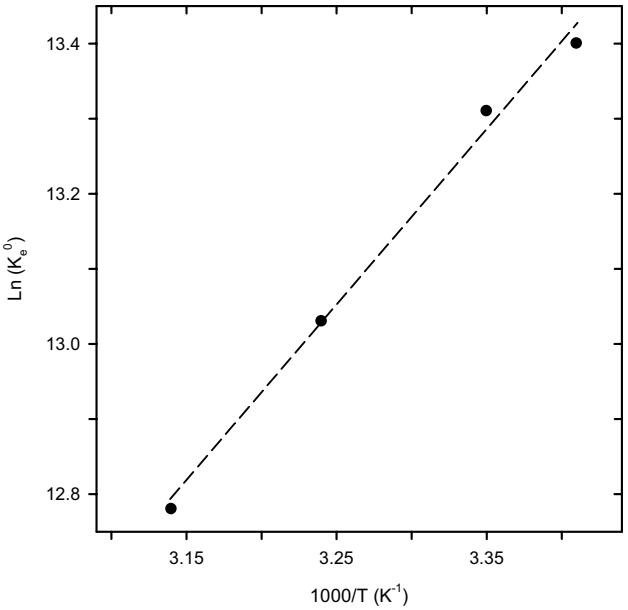

Fig. 10 Thermodynamic study for the MB adsorption on the clay sample, performed through fitting of the experimental data to the linear form of van't Hoff equation

Table 7 Equilibrium constants based on the Langmuir isotherm and after applying Eq. (2) to make it dimensionless and values of Gibbs's free energy calculated from Eq. (1)

T (K)	K_L (L mg^{-1})	K_L (L mol^{-1})	K_e°	Ln (K_e°)	$\Delta G°$ (kJ mol^{-1})
293	2.06	65.78×10^4	65.78×10^4	13.40	− 32.71
298	1.89	60.45×10^4	60.45×10^4	13.31	− 32.94
308	1.41	45.20×10^4	45.20×10^4	13.02	− 33.34
318	1.11	35.54×10^4	35.54×10^4	12.78	− 33.70

the recovery of intensity of the bands located in the upper region, reasonably due to rehydration of the calcined clay that constitutes the matrix of the monolith under the aqueous medium treatment.

The recirculated plug-flow tests were performed using two initial concentrations of MB, 20 and 100 mg L^{-1}, in aqueous solution, and also employing a column containing the same quantity of clay in the form of powder and calcined at the same temperature as the monolith for comparative purposes. Figure 11 shows the results obtained in this study. As can be noticed, the adsorptive behavior changes with the initial concentration of the adsorbate. For low concentrations of MB ($C_0 = 20$ mg L^{-1}), the differences observed between the two samples studied, honeycomb monolith and packed column, are relatively small. The maximum quantities of pollutant absorbed by the two samples are 2.8 and 2.9 mg g^{-1}, respectively. The obtained curves also show that the elimination of pollutant is almost complete after 3 h of flow recirculation under the tested experimental conditions. On the contrary, the experiments carried out for higher concentration of MB ($C_0 = 100$ mg L^{-1}) allow a clearer differentiation between the two studied samples. The clay-based monolith becomes more efficient adsorbent than the column. Although total elimination of MB cannot be achieved after 500 min of flow, the removal efficiency varies from about 41% for the clay-based monolith to 37% for the column that contains the same quantity of powdered clay. These results correspond to an adsorbed amount of 5.9 and 5.1 mg g^{-1}, respectively. Moreover, experiments of much longer duration (not shown) indicated that after 24 h the monolith and the packed column adsorbed 9.1 and 7.2 mg/g, respectively, confirming the higher removal efficiency of the former (58% vs 48% in the case of the column). These experiments also demonstrated the reproducibility of the results obtained up to 8 h, with an experimental deviation lower than 2%.

It is also noteworthy that in the case of the packed column the flow measured at the outlet was immediately decreased from 1200 to 400 cm^3 min^{-1}, whereas the flow kept constant during the whole experiment in the case of the monolith. This observation has a double significance. First, it demonstrates the advantage of using the honeycomb monolith to avoid pressure drop problems, a virtue that joins that of easy replacement upon saturation. Second, it gives double value to the results obtained with this design because it operated under less favored conditions for adsorption such as a three times lower contact time than that employed for the packed powder [15]. Moreover, the results obtained with the clay monoliths of this study are also more interesting than those we previously observed for similar clay honeycomb monoliths that even had been activated by means of coal templating, measuring under the same experimental conditions [36].

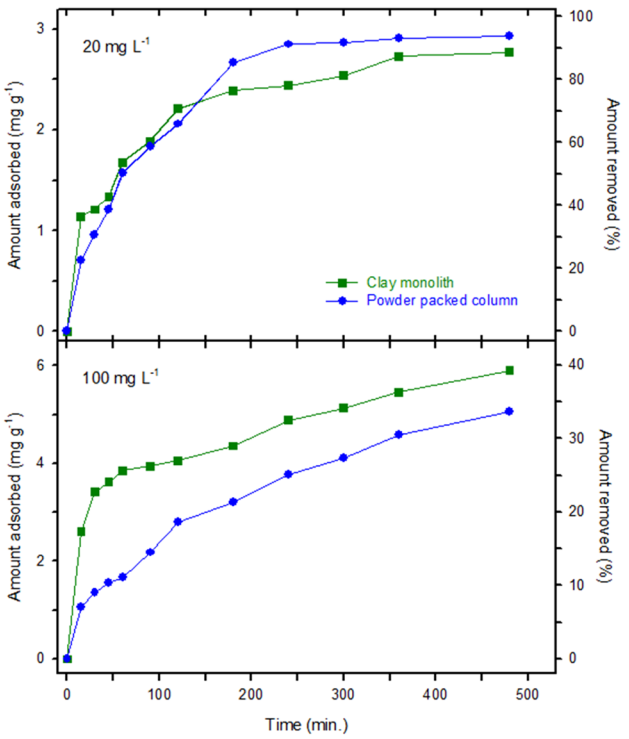

Fig. 11 Methylene blue adsorption at room temperature as a function of time on the clay honeycomb monolith and a packed column containing the same amount of calcined clay

4 Conclusion

According to textural, chemical and structural characterization, the studied raw argillaceous material mainly consisted of a thermally stable interstratified illite–smectite with appropriate porosity and surface area for use as adsorbent. Its maximum methylene blue (MB) adsorption capacity was found to be 100 mg g^{-1} at 45 °C. The adsorption isotherms of MB dye could be satisfactorily described by the equations of Langmuir model. The kinetic study of the MB retention by the clay revealed that the adsorption process is of second order, while the thermodynamic study indicated its exothermic character and spontaneity in the range from 20 to 45 °C.

The results obtained with honeycomb monoliths extruded from this clay without additives were of particular interest. They proved that the application of structured filters under dynamic conditions could be more effective than using packed columns of the same material but in powdered form. For example, the integral clay honeycomb monoliths allowed almost complete removal of MB from

1 L of aqueous solution containing 20 mg L^{-1} of MB, in recirculating flow experiments and for relatively short times (< 6 h), operating with 6.5 g weighted monoliths at 1200 cm^3 min^{-1}.

Acknowledgements Financial support from the MINECO-Spain/FEDER (MAT2017-87579-R and MAT2017-84228-R Projects) and the Junta de Andalucía (FQM-110 group). M. Ahrouch is grateful for its AUE-UCA fellowship. We acknowledge the electron microscopy and X-ray diffraction divisions of the SC-ICyT of University of Cádiz, and Dr. G.A. Cifredo for his help in the XRD analysis.

Compliance with ethical standards

Conflict of interest The author(s) declare that they have no competing interests.

References

1. Benguella B, Yacouta-Nour A (1999) Elimination des colorants acides en solution aqueuse par la bentonite et le kaolin. C R Chimie 12:762–771. https://doi.org/10.1016/j.crci.2008.11.008
2. Zollinger H (1987) Color Chemistry-Synthesis, Properties and Application of Organic Dyes and pigments. VCH Publishers, New York. https://doi.org/10.1002/anie.200385122
3. Errais E, Duplay J, Darragi F, M'Rabet I, Aubert A, Huber F, Morvan G (2011) Efficient anionic dye adsorption on natural untreated clay: kinetic study and thermodynamic parameters. Desalination 275:74–81. https://doi.org/10.1016/j.desal.2011.02.031
4. Souabi S, Yaacoubi A, Frouji A, Yacoubi A, Belkhadir EM (1996) Etude de l'elimination des colorants des rejets de l'industrie textile. Tech Sci Méthodes 3:181–185
5. Netpradit S, Thiravetyan P, Towprayoon S (2004) Adsorption of three azo reactive dyes by metal hydroxide sludge: effect of temperature, pH, and electrolytes. J Colloid Interface Sci 270:255–261. https://doi.org/10.1016/j.jcis.2003.08.073
6. Mottaleb M, Littlejohn D (2001) Application of an HPLC e FTIR modified thermospray interface for analysis of dye samples. Anal Sci 17:429–434
7. Arami M, Limaee NY, Mahmoodi NM, Tabrizi NS (2006) Equilibrium and kinetics for the adsorption of direct and acid dyes from aqueous solution by soy meal hull. J Hazard Mater 135:171–179. https://doi.org/10.1016/j.jhazmat.2005.11.044
8. Fernandes AN, Almeida CAP, Menezes CTB, Debacher NA, Sierra MMD (2007) Removal of methylene blue from aqueous solution by peat. J Hazard Mater 144:412–419. https://doi.org/10.1016/j.jhazmat.2006.10.053
9. Bagane M, Guiza S (2000) Elimination d'un colorant des Effluents de l'industrie textile par adsorption. Ann Chim Sci Mat 25:615–626
10. Gupta GS, Prasad G, Singh VN (1990) Removal of chrome dye from aqueous solutions by mixed adsorbents fly ash and coal. Water Res 24:45–50. https://doi.org/10.1016/0043-1354(90)90063-C
11. Dali-Youcef Z, Bouabdasselem H, Bettahar N (2006) Élimination des composés organiques par des argiles locales. C R Chimie 9(10):1295–1300. https://doi.org/10.1016/j.crci.2006.05.001
12. Akar T, Demir TA, Kiran I, Özcan A, Özcan AS, Tunali S (2006) Biosorption potential of Neurospora crassa cells for decolorization of Acid Red 57 (AR57) dye. J Chem Technol Biotechnol 81:1100–1106. https://doi.org/10.1002/jctb.1462
13. Azharul Islam Md, Sabar S, Benhouria A, Khanday WA, Asif M, Hameed BH (2017) Nanoporous activated carbon prepared from karanj (*Pongamia pinnata*) fruit hulls for methylene blue adsorption. J Taiwan Inst Chem Eng 74:96–104. https://doi.org/10.1016/j.jtice.2017.01.016
14. Cheng S, Zhang L, Ma A, Xia H, Peng J, Li C, Shu J (2018) Comparison of activated carbon and iron/cerium modified activated carbon to remove methylene blue from wastewater. J Environ Sci 65:92–102. https://doi.org/10.1016/j.jes.2016.12.027
15. Pang J, Fu F, Ding Z, Lu J, Li N, Tang B (2017) Adsorption behaviors of methylene blue from aqueous solution on mesoporous birnessite. J Taiwan Inst Chem Eng 77:168–176. https://doi.org/10.1016/j.jtice.2017.04.041
16. Shakoor S, Nasar A (2016) Removal of methylene blue from artificially contaminated water using citrus limetta peel waste as very low cost adsorbent. J Taiwan Inst Chem Eng 66:154–163. https://doi.org/10.1016/j.jtice.2016.06.009
17. Bentahar Y, Draoui K, Hurel C, Ajouyed O, Khairoun S, Marmier N (2019) Physico-chemical characterization and valorization of swelling and non-swelling Moroccan clays in basic dye removal from aqueous solutions. J Afr Earth Sci 154:80–88. https://doi.org/10.1016/j.jafrearsci.2019.03.017
18. Rida K, Bouraoui S, Hadnine S (2013) Adsorption of methylene blue from aqueous solution by kaolin and zeolite. Appl Clay Sci 83–84:99–105. https://doi.org/10.1016/j.clay.2013.08.015
19. Chen P, Cao Z, Wen X, Wang J, Yang F, Qiu P, Yue Y, Liu G, Wang S, Zhong H (2017) A novel mesoporous silicate material (MS) preparation from dolomite and enhancing methylene blue removal by electronic induction. J Taiwan Inst Chem Eng 80:128–136. https://doi.org/10.1016/j.jtice.2017.08.044
20. El Mouzdahir Y, Elmchaouri A, Mahboub R, Gil A, Korili SA (2007) Adsorption of methylene blue from aqueous solutions on a Moroccan clay. J Chem Eng Data 52:1621–1625. https://doi.org/10.1021/je700008g
21. Shaban M, Abukhadra MR, Khan AAP, Jibali BM (2018) Removal of Congo red, methylene blue and Cr(VI) ions from water using natural serpentine. J Taiwan Inst Chem Eng 82:102–116. https://doi.org/10.1016/j.jtice.2017.10.023
22. Zhang Z, Wang W, Wang A (2015) Highly effective removal of methylene blue using functionalized attapulgite via hydrothermal process. J Environ Sci 33:106–115. https://doi.org/10.1016/j.jes.2014.12.014
23. Gatica JM, Vidal H (2010) Non-cordierite clay-based structured materials for environmental applications. J Hazard Mater 181:9–18. https://doi.org/10.1016/j.jhazmat.2010.05.041
24. Gatica JM, Vidal H (2011) Chapter 7 Use of clays to manufacture honeycomb monoliths for pollution control applications. In: Humphrey JP, Boyd DE (eds) Clay: types; properties and uses. Nova Science Publishers, New York, pp 253–273
25. Ahrouch M, Gatica JM, Draoui K, Bellido D, Vidal H (2019) Lead removal from aqueous solution by means of integral natural clays honeycomb monoliths. J Hazard Mater 365:519–530. https://doi.org/10.1016/j.jhazmat.2018.11.037
26. Chandrasekhar S, Pramada PN (2006) Rice husk as an adsorbent for methylene blue- effect of ashing temperature. Adsorption 12:27–43. https://doi.org/10.1007/s10450-006-0136-1
27. El Qada EN, Allen SJ, Walker GM (2006) Adsorption of methylene blue onto activated carbon produced from steam activated bituminous coal: a study of equilibrium adsorption isotherm. Chem Eng J 124:103–110. https://doi.org/10.1016/j.cej.2006.08.015
28. Almeida CAP, Debacher NA, Downs AJ, Cottet L, Mello CAD (2009) Removal of methylene blue from colored effluents by adsorption on montmorillonite clay. J Colloid Interface Sci 332(1):46–53. https://doi.org/10.1016/j.jcis.2008.12.012
29. Hamdaoui O (2006) Batch study of liquid-phase adsorption of methylene blue using cedar sawdust and crushed brick. J

Hazard Mater 135:264–273. https://doi.org/10.1016/j.jhazmat.2005.11.062
30. Mohammed MA, Shitu A, Ibrahim A (2014) Removal of methylene blue using low cost adsorbents: a review. Res J Chem Sci 4(1):91–102
31. Rafatullah M, Sulaiman O, Hashim R, Ahmad A (2010) Adsorption of methylene blue on low-cost adsorbents: a review. J Hazard Mater 177:70–80. https://doi.org/10.1016/j.jhazmat.2009.12.047
32. Ciesielski H, Sterckeman T (1997) Determination of cation exchange capacity and exchangeable cations in soils by means of cobalt hexamine trichloride. Effects of experimental conditions. Agronomie 17:1–7. https://doi.org/10.1051/agro:19970101
33. Hang PT, Brindley GW (1970) Methylene blue adsorption by clay minerals. Determination of surface areas and cation exchange capacities (clay-organic studies XVIII). Clays Clay Minerals 18(4):203–212
34. Cottet L, Almeida CAP, Naidek N, Viante MF, Lopes MC, Debacher NA (2014) Adsorption characteristics of Montmorillonite clay modified with iron oxide with respect to methylene blue in aqueous media. Appl Clay Sci 95:25–31. https://doi.org/10.1016/j.clay.2014.03.023
35. Gatica JM, Rodríguez-Izquierdo JM, Sánchez D, Ania C, Parra JB, Vidal H (2004) Extension of preparation methods employed with ceramic materials to carbon honeycomb monoliths. Carbon 42:3252–3254. https://doi.org/10.1016/j.carbon.2004.06.040
36. Cifredo G, Gatica JM, Harti S, Vidal H (2010) Easy route to activate clay honeycomb monoliths for environmental applications. Appl Clay Sci 47:392–399. https://doi.org/10.1016/j.clay.2009.12.003
37. Rodríguez-Carvajal JJ (1993) Recent advances in magnetic structure determination by neutron power diffraction. Phys B 192:55–69. https://doi.org/10.1016/0921-4526(93)90108-I
38. Ho YS (2004) Citation review of Langergren kinetic rate equation on adsorption reactions. Scientometrics 59:171–177
39. Wang L, Wang A (2008) Adsorption properties of Congo red from aqueous solution onto surfactant-modified montmorillonite. J Hazard Mater 160:173–180. https://doi.org/10.1016/j.jhazmat.2008.02.104
40. Chafik T, Harti S, Cifredo G, Gatica JM, Vidal H (2009) Easy extrusion of honeycomb-shaped monoliths using Moroccan natural clays and investigation of their dynamic adsorptive behaviour towards VOCs. J Hazard Mater 170:87–95. https://doi.org/10.1016/j.jhazmat.2009.04.127
41. Harti S, Cifredo G, Gatica JM, Vidal H, Chafik T (2007) Physicochemical characterization and adsorptive properties of some Moroccan clay minerals extruded as lab-scale monoliths. Appl Clay Sci 36:287–296. https://doi.org/10.1016/j.clay.2006.10.004
42. Acemana S, Lahav N, Yariv S (1999) A thermo-FTIR spectroscopy analysis of Al-pillared smectites differing in source of charge, in KBr disks. Thermochim Acta 340–341:349–366. https://doi.org/10.1016/S0040-6031(99)00281-6
43. Hadri M, Chaouki Z, Zaitan H, Draoui K, Barhoun A, Nawdali M, Valdés H, Drouiche N (2017) Adsorption of a cationic dye from aqueous solution using low-cost Moroccan diatomite: adsorption equilibrium, kinetic and thermodynamic studies. Desalin Water Treat 75:213–224. https://doi.org/10.5004/dwt.2017.20553
44. Vázquez T, Blanco MT (1981) Tabla de frecuencias y espectros de absorción infrarroja de compuestos relacionados con la química del cemento. Mater Constr 182:31–48. https://doi.org/10.3989/mc.1981.v31.i182.1007
45. Ríos-León I, Solano-Pola C, Rodríguez-Ruiz J, Espinosa-Fuentes E, Meza-Fuentes E (2017) Study by infrared spectroscopy and thermogravimetry of the effect of temperature on nickel-aluminum hydrotalcites. DYNA 84(201):9–16. https://doi.org/10.15446/dyna.v84n201.59768
46. Sing KSW, Everett DH, Haul RAW, Moscou L, Pierotti RA, Rouquérol J, Siemieniewska T (1985) Reporting physisorption data for gas/solid systems with special reference to the determination of surface area and porosity. Pure Appl Chem 57(4):603–619. https://doi.org/10.1351/pac198557040603
47. Elmoubarki R, Mahjoubi FZ, Tounsadi H, Moustadraf J, Abdennouri M, Zouhri A, El Albani A, Barka H (2015) Adsorption of textile dyes on raw and decanted Moroccan clays: kinetics, equilibrium and thermodynamics. Water Resour Ind 9:16–29. https://doi.org/10.1016/j.wri.2014.11.001
48. Namasivayam C, Sureshkumar MV (2006) Anionic dye adsorption characteristics of surfactant modified coir pith, a waste lignocellulosic polymer. J Appl Polym Sci 100:1538–1546. https://doi.org/10.1002/app.23278
49. Sureshkumar MV, Namasivayam C (2008) Adsorption behavior of Direct Red 12B and Rhodamine B from water onto surfactant-modified coconut coir pith. Colloid Surf A 317:277–283. https://doi.org/10.1016/j.colsurfa.2007.10.026
50. Doğan M, Özdemir Y, Alkan M (2007) Adsorption kinetics and mechanism of cationic methyl violet and methylene blue dyes onto sepiolite. Dyes Pigm 75(3):701–713. https://doi.org/10.1016/j.dyepig.2006.07.023
51. Giles CH, MacEvan TH, Nakhua SN, Smith D (1960) Studies on adsorption-XI. J Chem Soc 111:3973–3993
52. Giles CH, D'Silva AP, Easton IA (1974) A general treatment and classification of the solute adsorption isotherm. II. Experimental interpretation. J Colloid Interface Sci 47(3):766–778
53. Lima EC, Hosseini-Bandegharaei A, Moreno-Piraján JC, Anastopoulos I (2019) A critical review of the estimation of the thermodynamic parameters on adsorption equilibria. Wrong use of equilibrium constant in the Van't Hoof equation for calculation of thermodynamic parameters of adsorption. J Mol Liq 273:425–434. https://doi.org/10.1016/j.molliq.2018.10.048
54. Liu Y (2009) Is the free energy change of adsorption correctly calculated? J Chem Eng Data 54:1981–1985. https://doi.org/10.1021/je800661q
55. Auta M, Hameed BH (2012) Modified mesoporous clay adsorbent for adsorption isotherm and kinetics of methylene blue. Chem Eng J 198–199:219–227. https://doi.org/10.1016/j.cej.2012.05.075
56. Omer OS, Hussein MA, Hussein BHM, Mgaidi A (2018) Adsorption thermodynamics of cationic dyes (methylene blue and crystal violet) to a natural clay mineral from aqueous solution between 293.15 and 323.15 K. Arab J Chem 11(5):615–623. https://doi.org/10.1016/j.arabjc.2017.10.007
57. Ovchinnikov OV, Evtukhova AV, Kondratenko TS, Smirnov MS, Khokhlov VY, Erina OV (2016) Manifestation of intermolecular interactions in FTIR spectra of methylene blue molecules. Vibr Spectrosc 86:181–189. https://doi.org/10.1016/j.vibspec.2016.06.016